



**University of  
Zurich**<sup>UZH</sup>

**Zurich Open Repository and  
Archive**

University of Zurich  
University Library  
Strickhofstrasse 39  
CH-8057 Zurich  
[www.zora.uzh.ch](http://www.zora.uzh.ch)

---

Year: 2024

---

## **Summer drought weakens land surface cooling of tundra vegetation**

Rietze, Nils ; Assmann, Jakob J ; Plekhanova, Elena ; Naegeli, Kathrin ; Damm, Alexander ; Maximov, Trofim C ;  
Karsanaev, Sergey V ; Hensgens, Geert ; Schaepman-Strub, Gabriela

DOI: <https://doi.org/10.1088/1748-9326/ad345e>

Posted at the Zurich Open Repository and Archive, University of Zurich

ZORA URL: <https://doi.org/10.5167/uzh-259081>

Journal Article

Published Version



The following work is licensed under a Creative Commons: Attribution 4.0 International (CC BY 4.0) License.

Originally published at:

Rietze, Nils; Assmann, Jakob J; Plekhanova, Elena; Naegeli, Kathrin; Damm, Alexander; Maximov, Trofim C; Karsanaev, Sergey V; Hensgens, Geert; Schaepman-Strub, Gabriela (2024). Summer drought weakens land surface cooling of tundra vegetation. *Environmental Research Letters*, 19(4):044043.

DOI: <https://doi.org/10.1088/1748-9326/ad345e>

ENVIRONMENTAL RESEARCH  
LETTERS

## LETTER

Summer drought weakens land surface cooling of tundra  
vegetation

## OPEN ACCESS

## RECEIVED

1 September 2023

## REVISED

20 December 2023

## ACCEPTED FOR PUBLICATION

15 March 2024

## PUBLISHED

22 March 2024

Original content from  
this work may be used  
under the terms of the  
[Creative Commons  
Attribution 4.0 licence](#).

Any further distribution  
of this work must  
maintain attribution to  
the author(s) and the title  
of the work, journal  
citation and DOI.



Nils Rietze<sup>1,2,\*</sup> , Jakob J Assmann<sup>1</sup> , Elena Plekhanova<sup>1</sup> , Kathrin Naegeli<sup>2</sup> , Alexander Damm<sup>2,3</sup> ,  
Trofim C Maximov<sup>4</sup>, Sergey V Karsanaev<sup>4</sup> , Geert Hensgens<sup>5</sup> , and Gabriela Schaepman-Strub<sup>1,\*</sup> 

<sup>1</sup> Department of Evolutionary Biology and Environmental Studies, University of Zurich, Zurich, Switzerland

<sup>2</sup> Department of Geography, University of Zurich, Zurich, Switzerland

<sup>3</sup> Eawag, Swiss Federal Institute of Aquatic Science and Technology, 8600 Dübendorf, Switzerland

<sup>4</sup> Institute for Biological Problems of the Cryolithozone, Siberian Branch Russian Academy of Sciences, Yakutsk, Russia

<sup>5</sup> Department of Earth and Climate, Vrije Universiteit Amsterdam, Amsterdam, The Netherlands

\* Authors to whom any correspondence should be addressed.

E-mail: [nils.rietze@uzh.ch](mailto:nils.rietze@uzh.ch) and [gabriela.schaepman@ieu.uzh.ch](mailto:gabriela.schaepman@ieu.uzh.ch)

**Keywords:** Arctic, tundra, drought, Siberia, land surface temperature, drones, heatwave

Supplementary material for this article is available [online](#)

**Abstract**

Siberia experienced a prolonged heatwave in the spring of 2020, resulting in extreme summer drought and major wildfires in the North-Eastern Siberian lowland tundra. In the Arctic tundra, plants play a key role in regulating the summer land surface energy budget by contributing to land surface cooling through evapotranspiration. Yet we know little about how drought conditions impact land surface cooling by tundra plant communities, potentially contributing to high air temperatures through a positive plant-mediated feedback. Here we used high-resolution land surface temperature and vegetation maps based on drone imagery to determine the impact of an extreme summer drought on land surface cooling in the lowland tundra of North-Eastern Siberia. We found that land surface cooling differed strongly among plant communities between the drought year 2020 and the reference year 2021. Further, we observed a decrease in the normalized land surface cooling (measured as water deficit index) in the drought year 2020 across all plant communities. This indicates a shift towards an energy budget dominated by sensible heat fluxes, contributing to land surface warming. Overall, our findings suggest significant variation in land surface cooling among common Arctic plant communities in the North-Eastern Siberian lowland tundra and a pronounced effect of drought on all community types. Based on our results, we suggest discriminating between functional tundra plant communities when predicting the drought impacts on energy flux related processes such as land surface cooling, permafrost thaw and wildfires.

**1. Introduction**

In 2020, the North-Eastern Siberian tundra was exposed to a severe summer heatwave (Overland and Wang 2021) and extreme drought, as indicated by the global drought monitor (Beguería *et al* 2010). Simultaneously, this region experienced an unusually high number of wildfires that burned approximately 170 000 ha (Talucci *et al* 2022). The Arctic tundra is increasingly exposed to such extreme events, yet little is known about their impacts on plant communities (Walsh *et al* 2020, van Beest *et al* 2022).

Improved understanding of how tundra plant communities respond to drought is therefore crucial for improving our predictions of changes in ecosystem functions under future climate with more extremes.

Tundra vegetation regulates the summer land surface energy budget by controlling latent heat fluxes through evapotranspiration (Juszak *et al* 2016, Nedbal *et al* 2020, Oehri *et al* 2022). Vegetated areas moderate the surface heating and feed back to small-scale land surface cooling (Nedbal *et al* 2020), called plant thermoregulation (Still *et al* 2019). However, heatwaves and droughts may weaken this cooling

effect and create a sensible heat flux dominance, further intensifying the heatwave, such as during the 2010 heatwave and drought in western Siberia (Hauser *et al* 2016). Most studies linking land surface energy budgets with soil moisture relied on a few point measurements from flux chambers or towers (Marchand *et al* 2006, Thunberg *et al* 2021, Zona *et al* 2022). Yet, we have limited knowledge of how the effect of drought on land surface cooling varies across space at landscape and regional scales in the tundra biome (Farella *et al* 2022, Yang *et al* 2022).

One can estimate the variation of ecosystem functions and land surface energy fluxes using remotely sensed land surface temperature ( $T_{\text{surf}}$ ) (Still *et al* 2019, Nedbal *et al* 2020, Kelly *et al* 2021, Farella *et al* 2022). Land surface cooling can be approximated by the surface-to-air temperature difference, which was used to quantify the canopy cooling ability in the Alaskan tundra under non-stressed conditions (Yang *et al* 2021). During heatwaves and droughts, this land surface cooling can weaken because of environmental factors, like a reduction in soil moisture supply (Farella *et al* 2022), or because of the physiological reaction of plants, closing their stomata to avoid excessive water loss (Katul *et al* 2012, Still *et al* 2019). The small-scale heterogeneity of tundra vegetation complicates the advancement of process understanding from the plant to the ecosystem level, since the spatial resolution of current space-borne thermal infrared (TIR) sensors covering the high latitudes is too low (Nill *et al* 2019, Yang *et al* 2021).

Recent advances in drone technology allows the detection of thermal properties at scales relevant to tundra ecosystems (Berni *et al* 2009, Faye *et al* 2016, Yang *et al* 2020). Drone data has been used to reveal substantial heterogeneity in the thermal properties and thus ecosystem functions of tundra plants (Yang *et al* 2021) and boreal wetlands (Kelly *et al* 2021). Consequently, drone-based TIR imagery is ideally suited to capture spatial variations in drought responses of tundra vegetation.

Here, we used indicators of land surface cooling based on high-resolution drone imagery and field observations to assess how Arctic plant communities responded to the 2020 summer drought at three study sites in the Indigirka lowlands of North-Eastern Siberia. First, we investigated how surface-to-air temperature differences ( $T_{\text{surf}} - T_{\text{air}}$ ) varied between the plant communities. Second, we analyzed how the drought impacted land surface cooling using the water deficit index (WDI). Third, we tested how the drought impact varied across different compositions of tundra plant communities. Overall, our study allows us to detect which plant communities in the study region might be most susceptible to the effects of drought and subsequent disturbances like permafrost thaw and wildfires.

## 2. Materials and methods

### 2.1. Study area

This study focuses on three Arctic tundra landscapes at the Kytalyk research station (70°49'N, 147°29'E), located in the continuous, ice-rich permafrost zone of the Indigirka lowlands in the Sakha Republic, Russia (figure 1). We conducted drone surveys as part of the data collection for the High Latitude Drone Ecology Network (see common protocol on <https://arcticdrones.org/>) and studied three areas based on subsets of 400 m × 400 m (0.16 km<sup>2</sup>, see figure 1) covered by drone flights in both years.

The three study sites are characterized by different landforms capturing the common vegetation types: (1) a drained thaw lake basin (TLB) with shrub or lichen-dominated high-centered polygons and wet sedge-dominated low-centered polygons, (2) tussock-sedge dominated Yedomas hills (Ridge), and (3) a transitional zone with thermokarst ponds, shrub-dominated high-centered polygons, and low-centered wetland complexes characterized by wet sedges at the bottom and moss dominated mounds with patches of cloudberry *Rubus chamaemorus* L., henceforth Cloudberry Hills (CBH).

### 2.2. Meteorological conditions

The weather and drought conditions differed notably between the drought year (2020) and the reference year (2021) (table 1, figure S3). While total summer (JJA) precipitation at the meteorological station in Chokurdakh, located approximately 30 km from the study site, fell below average in 2020 (figure S1(a)), the mean summer air temperature (figure S1(b)) in both years exceeded the 90th percentile and ranked second (2020) and fourth (2021) in the entire record (1945–2021, Kazakov (2023)). We defined the drought status using the multi-month standardized precipitation evapotranspiration index (SPEI) (Vicente-Serrano *et al* 2010) using the Chokurdakh time series. The 3 month SPEI (SPEI<sub>3</sub>) between June to August 2020 was below the 10th percentile (−1.37) and reached −2.94 in July 2020, indicating an extreme drought (*sensu* Slette *et al* (2019)) (table 1, figure S2). In July 2021, the SPEI<sub>3</sub> was within minus one and one (−0.26, table 1), indicating ‘near normal’ conditions (*sensu* Slette *et al* (2019)). We also observed a drop in the normalized difference vegetation index between the reference year (2021) and the drought year (2020) in the drone imagery (figure S4).

For our analysis of drought impact on land surface cooling, we used local, short-term mean air temperatures from a temperature sensor (Barani Design Technologies s.r.o, Bratislava, Slovakia) installed at 2 m above ground on a flux tower close to the research station. This flux tower is situated ca. 500 m from the center of the TLB, 670 m from the CBH, and 1000 m from the Ridge site. A similar composition of

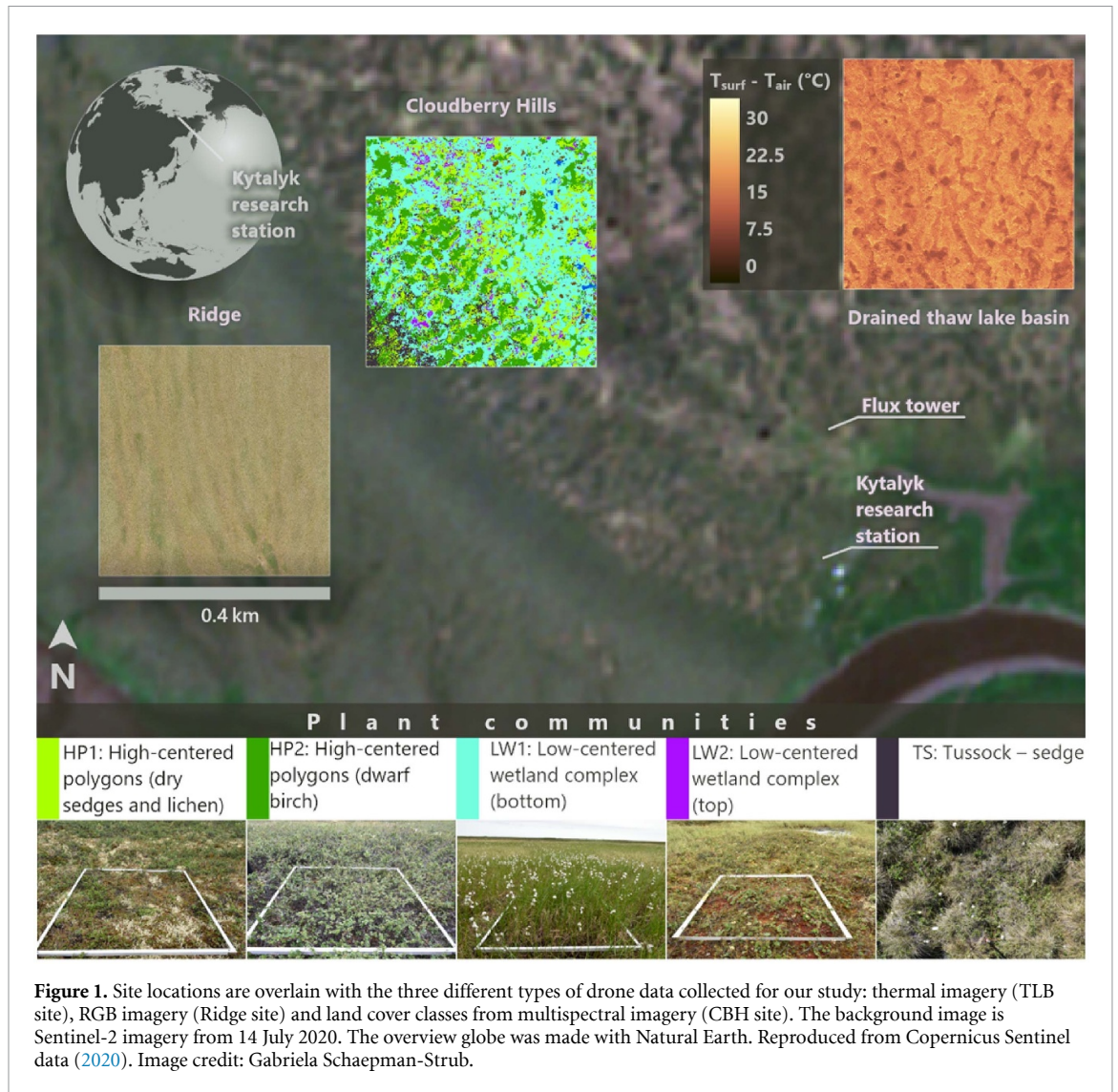


**Figure 1.** Site locations are overlain with the three different types of drone data collected for our study: thermal imagery (TLB site), RGB imagery (Ridge site) and land cover classes from multispectral imagery (CBH site). The background image is Sentinel-2 imagery from 14 July 2020. The overview globe was made with Natural Earth. Reproduced from Copernicus Sentinel data (2020). Image credit: Gabriela Schaeppman-Strub.

**Table 1.** The mean surface ( $T_{\text{surf}}$ ) temperature at the study sites, nearby air temperature ( $T_{\text{air}}$ ), incoming shortwave radiation ( $SW_{\text{in}}$ ), and standardized precipitation evapotranspiration index (SPEI) differed between the flight campaigns in 2020 (drought year) and 2021. Interestingly, the Ridge site showed a cooler  $T_{\text{surf}}$  than  $T_{\text{air}}$  in 2020, which is further discussed in the supplementary materials section 1. The mean  $T_{\text{air}}$  and  $SW_{\text{in}}$  were derived from a flux tower located ca. 500–1000 m from the centers of the study sites. Values represent the mean between the take-off and landing of the drone surveys covering the study sites on the respective dates. The local times for take-off and landing are given. SPEI<sub>3</sub> and SPEI<sub>6</sub> represent the drought severity during the month of the flights. For more detailed local weather conditions see figure S4. The site acronyms are CBH = Cloudberry Hills and TLB = drained thaw lake basin.

Date	SPEI <sub>3</sub>	SPEI <sub>6</sub>	Site	Time of flight	Mean $T_{\text{surf}}$ (°C)	Mean $T_{\text{air}}$ (°C)	Mean wind speed (m s <sup>-1</sup> )	Mean $SW_{\text{in}}$ (W m <sup>-2</sup> )
24 July 2020	-2.94	-2.18	CBH	18:10–18:48	29.28	24.07	0.86	41.42
			Ridge	16:20–17:04	25.35	27.33	1.56	219.75
			TLB	17:25–17:57	28.58	26.12	1.40	55.88
19 July 2021	-0.26	-0.43	CBH	14:45–15:12	28.14	13.81	2.43	647.23
			Ridge	15:52–16:32	27.30	14.61	2.20	555.45
			TLB	13:57–14:26	29.48	13.30	2.02	667.65

landforms and plant communities to that of the TLB site surrounds the flux tower (Parmentier *et al* 2011). The incoming shortwave radiation was retrieved from a CMP21 pyranometer (OTT Hydromet B.V., Delft, Netherlands) installed on the flux tower ca. 1.5 m above ground.

### 2.3. Multispectral, thermal, and RGB imagery

We carried out drone surveys over all three sites on the same day during the peak growing season in 2020 and 2021, which resulted in six scenes per site with multispectral, RGB, and thermal imagery. We collected multispectral imagery to classify plant

communities using a MicaSense RedEdge-MX camera (MicaSense Inc., Seattle, WA, USA). To map land surface temperature ( $T_{\text{surf}}$ ), we acquired simultaneous TIR and RGB imagery using a senseFly DuetT camera (senseFly SA, Cheseaux-Lausanne, Switzerland). The thermal sensor (FLIR Tau 2 640, FLIR Systems Inc., Wilsonville, OR, USA) is uncooled and we did not deploy in-flight thermal calibration targets, limiting the absolute accuracy of our  $T_{\text{surf}}$  measurements. All sensors were mounted on a fixed-wing drone (eBee X, senseFly SA, Cheseaux-Lausanne, Switzerland). Detailed sensor specifications are listed in table S1, all data was made available on Zenodo (Rietze *et al* 2024).

## 2.4. Drone data preprocessing

### 2.4.1. Sensor drift correction

We observed a drift in the thermal sensor's internal temperature ( $T_{\text{sens}}$ ) during all thermal flights, consequently causing a drift in the recorded  $T_{\text{surf}}$  (figure S5). Due to the lack of thermal calibration targets, we were unable to correct the drift using a field-validated empirical model as suggested by Kelly *et al* (2019) and Mesas-Carrascosa *et al* (2018). Instead, we adapted the method by Mesas-Carrascosa *et al* (2018) using the relationship between  $T_{\text{sens}}$  and  $T_{\text{corr}}$  to derive an empirical drift correction function, where  $T_{\text{corr}}$  is the deviation of the mean  $T_{\text{surf}}$  of an individual image ( $\overline{T_{\text{surf}}}$ ) during the period of sensor instability (when  $T_{\text{sens}} > T_{\text{sens,min}} + 0.1$  °C) from the  $\overline{T_{\text{surf}}}$  during sensor stability. With this definition,  $T_{\text{corr}}$  is close to zero for images when the sensor was close to stable. First, we fitted quadratic models between  $T_{\text{sens}}$  and  $T_{\text{corr}}$  to determine  $T_{\text{corr}}$  for a given  $T_{\text{sens}}$ , following equation (1):

$$T_{\text{corr}} = a * T_{\text{sens}}^2 + b * T_{\text{sens}} + c. \quad (1)$$

The coefficient of determination ( $R^2$ ) of the fitted models ranged from 0.66 to 0.97 (figure S6, empirical coefficients in table S2) and for some images taken at high  $T_{\text{sens}}$ ,  $T_{\text{surf,raw}}$  had to be corrected by up to 10 °C (e.g. figure S6(a)). Second, we subtracted the correction temperature from the surface temperatures in the entire image (corrected images in figure S7):

$$T_{\text{surf}} = T_{\text{surf,raw}} - T_{\text{corr}}. \quad (2)$$

### 2.4.2. Geometric processing and orthomosaics

We used a virtual dGNSS reference station (senseFly GeoBase, senseFly SA, Cheseaux-Lausanne, Switzerland) and post-processed kinematics (PPK) to geolocate the drone imagery with a spatial accuracy of 1 cm and 3 cm for the multispectral and thermal imagery respectively (see supplementary materials). We aligned and processed the imagery using the photogrammetry software Pix4D Mapper (version 4.8.1, Pix4D SA, Prilly, Switzerland). Finally, we resampled all mosaics to an identical grid with a common resolution of 15 cm, which is close to the original

ground sampling distance of the thermal orthomosaics (14.1 cm to 15 cm).

## 2.5. Land cover classification

We classified the land cover at each site based on the 2021 multispectral drone imagery using a pixel-based random forest classifier (for details see supplementary materials section 2.2.4). We separated seven land cover types of which five represent different functional plant communities (see table 2). These communities are closely related to those used in the CircumArctic Vegetation Map (CAVM) (Raynolds *et al* 2019) but separated more specifically for our study on the hypothesis that they have distinct thermal characteristics. We applied a separate classification for each site, because not all plant communities were found at each site. We additionally classified open water and open mud in both years to avoid these pixels in the analysis of vegetation-related land surface cooling, and to allow a  $T_{\text{surf}} - T_{\text{air}}$  normalization over water surfaces (figure S8). We selected a total of ten spectral bands and indices for the classification based on the separability of their distributions (see table S3).

We generated training and validation data for the classification by manually outlining polygons for all three sites, guided by a set of plot-level RGB images taken with a handheld camera during the field campaign in 2021. In total, we defined 165 polygons across the three sites and sampled 200 pixels per polygon to ensure an even distribution of pixels across all vegetation communities. The resulting dataset of 33'000 pixels was split into a training (80%) and validation set (20%) stratified by polygon to avoid mixing training and validation data within a polygon.

We trained the site-specific random forest models on the respective training sets and assessed the classification accuracies using cross-validated overall accuracy scores and confusion matrices (tables S4–S6). The overall cross-validated classification accuracy was 88% averaged over all three sites, ranging from 83% at the CBH site to 94% at the TLB site. The mean user's accuracies of individual study sites ranged from 90% at the CBH site to 99.5% at the Ridge site, the latter being almost uniformly covered by the tussock-sedge vegetation class. Finally, a  $5 \times 5$  pixel modal filter was applied to the classified maps to reduce salt and pepper noise from single-pixel plant communities.

## 2.6. Analysis of land surface cooling

We analyzed (1) the variation in land surface cooling across plant communities, (2) the change in normalized land surface cooling between years, and (3) the relation between drought response and mixtures of plant communities. For the first two analyses, we randomly sampled 20'000 pixels per community and study site to account for spatial autocorrelation.

**Table 2.** We classified the multispectral imagery into five classes representing plant communities and two non-vegetated classes (mud and water, not shown in this table). Below, we present the species that dominate the canopy of the respective plant community.

Plant community	Description	Dominant species	Found in	Similar to CAVM class
LW1	Low-centered wetland complex (bottom)	Wet sedges ( <i>Carex aquatilis</i> Wahlenb., <i>Eriophorum angustifolium</i> Honck.), <i>Sphagnum</i> spp. L.	CBH, TLB, Ridge	W2
LW2	Low-centered wetland complex (top)	Cloudberries ( <i>Rubus chamaemorus</i> ), <i>Sphagnum</i> spp., <i>Rhododendron tomentosum</i> s. <i>tommentosum</i> (Stokes) Harmaja	CBH	W2
HP1	High-centered polygons (dry sedges and lichen)	Dry sedges ( <i>Carex bigelowii</i> s. <i>ensifolia</i> (Turcz. ex Ledeb.) ined.), fruticose lichen	CBH, TLB	G3
HP2	High-centered polygons (dwarf birch)	Dwarf birch ( <i>Betula nana</i> L.), <i>Sphagnum</i> spp., willows ( <i>Salix pulchra</i> Cham.)	CBH, TLB, Ridge	S1
TS	Tussock—sedge	Tussock sedges ( <i>Eriophorum vaginatum</i> L.)	CBH, Ridge	G4

### 2.6.1. Land surface cooling across Arctic plant communities

To investigate how the plant communities differ in their land surface cooling capacity, we calculated canopy-to-air temperature difference  $T_{\text{surf}} - T_{\text{air}}$  ( $\Delta T_{\text{surf-air}}$ ). Here,  $T_{\text{air}}$  represents the mean air temperature during the time of the flights from the 2 m flux tower temperature sensor. We tested for differences in  $\Delta T_{\text{surf-air}}$  among the plant communities in both years using Tukey's honest significance test (Tukey HSD), as this test accounts for all combinations of communities simultaneously.

To validate our analysis, we compared drone-based  $\Delta T_{\text{surf-air}}$  with  $\Delta T_{\text{surf-air}}$  derived from microclimatic observations of near-surface air temperatures from 28 TMS-4 loggers (TOMST s.r.o., Prague, Czech Republic) distributed in the TLB and Ridge sites in July 2021 (see supplementary materials section 3.1).

### 2.6.2. Comparison of the WDI between 2020 and 2021

The magnitudes and variations of  $\Delta T_{\text{surf-air}}$  differed between 2020 and 2021 owing to different cloud cover and windspeeds at the time of the drone flights (refer to figure S3 and the supplementary materials section 1.1 for a detailed description of the meteorological conditions). We therefore normalized  $\Delta T_{\text{surf-air}}$  using the WDI from Moran *et al* (1994) to compare the land surface cooling between the drought and reference year. The WDI is calculated separately for each year and site as follows:

$$\text{WDI} = \frac{\Delta T - \Delta T_{\text{min}}}{\Delta T_{\text{max}} - \Delta T_{\text{min}}} \quad (3)$$

where  $\Delta T$  is the observed  $\Delta T_{\text{surf-air}}$  described above,  $\Delta T_{\text{min}}$  is the minimum  $\Delta T_{\text{surf-air}}$  over freely evaporating surfaces, i.e. open water bodies, and  $\Delta T_{\text{max}}$  is the maximum  $\Delta T_{\text{surf-air}}$  in each thermal drone mosaic. The WDI values are therefore site-specific and we cannot compare WDI across sites. Values for the WDI typically range from 0 to 1, where 0 indicates strong land surface cooling close to the potential evapotranspiration rate of the surface, and 1 indicates weak land surface cooling. Hence, an increase in WDI would correspond to enhanced drought response of the vegetation canopy (Moran *et al* 1994). The WDI assumes a full canopy cover and that soil moisture is the dominant driver of surface temperature (Moran *et al* 1994), which holds true in the study sites. We investigated the inter-community and intra-community WDI differences using Tukey HSD and Welch's t-tests.

### 2.6.3. Analysis of drought response of tundra plant community mixtures

Lastly, we assessed if WDI differences ( $\Delta \text{WDI}$ ) between the two years were related to the mixture of plant communities in a given area. To this end, we determined the plant community composition in

grid cells covering an area of  $5\text{ m} \times 5\text{ m}$  by calculating the fractional cover (fCover) of each plant community in each grid cell from our land cover maps. We chose the 5 m resolution based on the variograms of the thermal orthomosaics and the study by Yang *et al* (2021). Fitted range sizes of the variogram models varied between 6.4 m for the Ridge site to 14.4 m in the TLB site (see figure S9), indicating that a resolution  $<6.4\text{ m}$  can capture the thermal heterogeneity at the sites. We assessed the influence of class fCover on the differences in WDI by fitting cubic curves to the fractional cover and  $\Delta\text{WDI}$  relationships for each vegetation type and evaluated the differences in responses qualitatively.

### 3. Results

#### 3.1. Differences in land surface cooling across plant communities in Kytalyk

We consistently detected lower land surface cooling (i.e. higher mean  $\Delta T_{\text{surf-air}}$ ) in high-centered polygons (HP) and tussock-sedge (TS) communities than in low-centered wetland complex communities (LW) during 2021 (figure 2) and 2020 (figure S10). The wet sedge and sphagnum-dominated communities (LW1) had the highest land surface cooling (i.e. lowest mean  $\Delta T_{\text{surf-air}}$ ) across all study sites and years, ranging between  $-2.2\text{ }^{\circ}\text{C}$  at the Ridge and  $4.6\text{ }^{\circ}\text{C}$  at the CBH site in 2020 (table S7), and between  $10.2\text{ }^{\circ}\text{C}$  at the Ridge and  $14.1\text{ }^{\circ}\text{C}$  at the drained TLB site in 2021 (figures 2 and S10). In contrast, tussock-sedges and lichen-dominated communities (HP1) generally had the lowest land surface cooling (i.e. highest mean  $\Delta T_{\text{surf-air}}$ ) (figure 2, tables S7 and S8). Mean  $\Delta T_{\text{surf-air}}$  in dwarf shrub-dominated communities (HP2), found in all three sites, ranged from  $-1.9\text{ }^{\circ}\text{C}$  at the Ridge to  $6.2\text{ }^{\circ}\text{C}$  at the CBH site in 2020 (table S7), and from  $12.2\text{ }^{\circ}\text{C}$  at the Ridge (figure 2(c)) to  $16.4\text{ }^{\circ}\text{C}$  at the TLB site (figure 2(b)) in 2021 (table S8). Even though mean  $\Delta T_{\text{surf-air}}$  was consistently higher in the reference year, the Tukey HSD tests revealed differences in the mean  $\Delta T_{\text{surf-air}}$  among all but three plant communities which persisted in both years (figure 2, tables S9 and S10). We observed the strongest differences in mean  $\Delta T_{\text{surf-air}}$  between wet sedge and sphagnum-dominated (LW1) and lichen-dominated communities (HP1) across the TLB and Ridge, reaching  $1.4\text{ }^{\circ}\text{C}$  in 2020 ( $p < 0.01$ , table S9) and  $3.6\text{ }^{\circ}\text{C}$  in 2021 ( $p < 0.01$ , table S10).

We observed comparable magnitudes of interquartile ranges (IQR spans from the 25% to 75% percentile) among communities. However, the variation of  $\Delta T_{\text{surf-air}}$  decreased strongly in the drought year, e.g. the IQR of wet-sedge and sphagnum-dominated communities (LW1) in the CBH site was  $3.2\text{ }^{\circ}\text{C}$  in 2021 but only  $2.3\text{ }^{\circ}\text{C}$  in 2020 (tables S7 and S8).

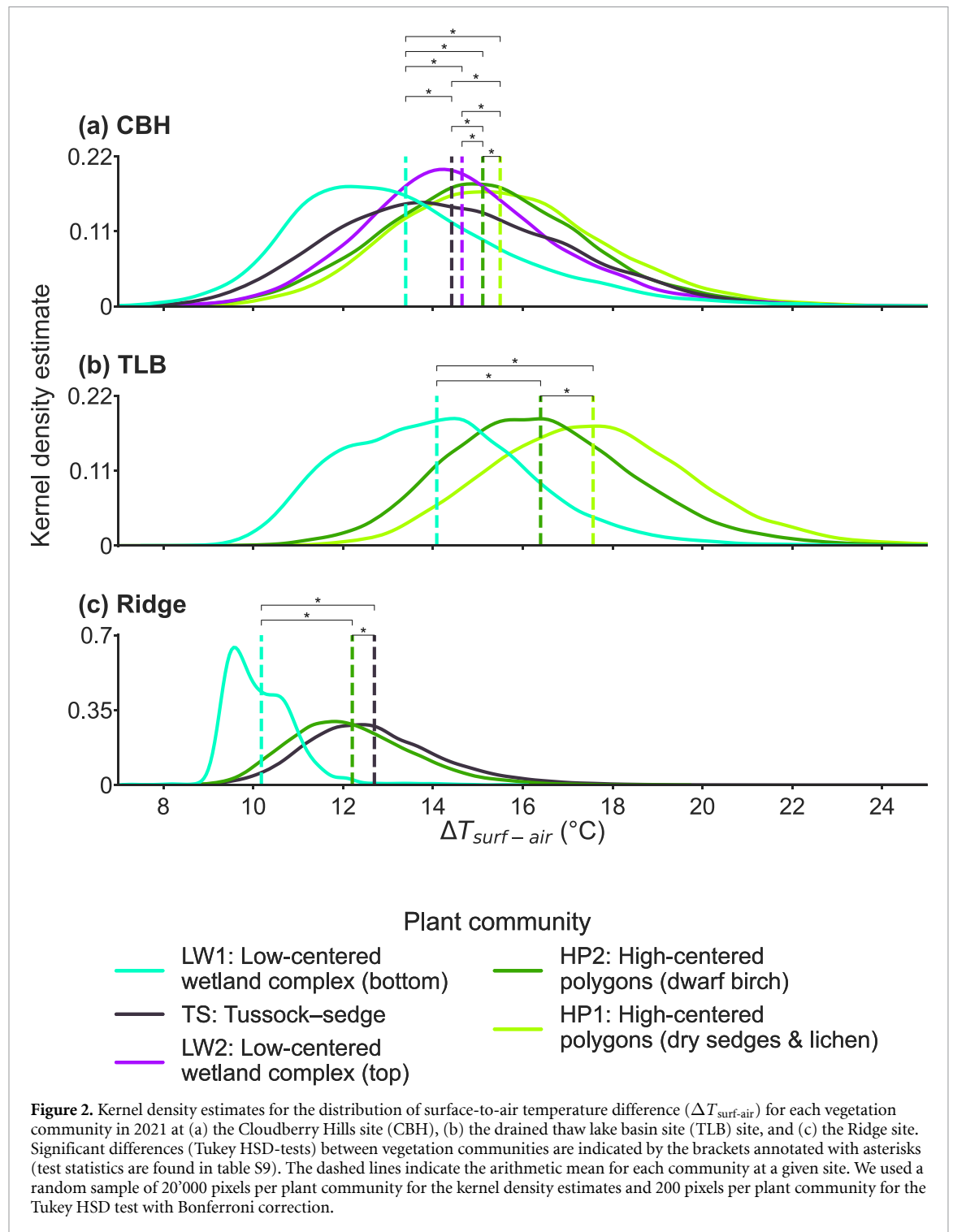
The in situ sensor TMS-4 and drone-derived  $\Delta T_{\text{surf-air}}$  showed consistent patterns when ranked by mean  $\Delta T_{\text{surf-air}}$  across communities during the 2021 drone flights (figure S11(a) and table S11). Although absolute values of TMS-4 derived  $\Delta T_{\text{surf-air}}$  were lower than the drone-derived  $\Delta T_{\text{surf-air}}$ , the consistent patterns suggest that drone data effectively captured in situ  $\Delta T_{\text{surf-air}}$  variation. This ranking was identical to the ranking of TMS-4 derived soil moisture counts, e.g. LW1 had a higher soil moisture count than HP2 and HP1 at the TLB site (figure S11(e)).

#### 3.2. Higher WDI under extreme drought conditions

The WDI was consistently higher during the extreme drought in 2020 for all plant communities (figures 3 and S12). The mean WDI increases between 2020 and 2021 were significant ( $p$ -values  $< 0.01$ ) and of similar magnitude ( $\sim 0.2$ ) across all plant communities, but strongest in HP2 communities (table S12). None of the interquartile ranges of WDI overlapped between 2020 and 2021 (figure 3 and table S13). The WDI was consistently low over open water surfaces at the CBH site in both years (figure 3), while retaining the differences among plant communities highlighted in section 3.1 (see results of the Tukey HSD test on the WDI in tables S14 and S15). For example, the wet sedge and sphagnum covered community (LW1) showed the lowest WDI of all plant communities, and the dwarf birch-dominated communities (HP2) remained higher across sites and years. Despite the similar increase in WDI, we detected strong spatial differences in the change of WDI among several plant communities (figure S13), e.g. the average WDI increase of the sphagnum and wet-sedge dominated communities (LW1) at the CBH site was lower than in dwarf birch-dominated communities (HP2) ( $-0.05$ ,  $p$ -value  $< 0.01$ , table S16).

#### 3.3. Integrating the drought response over plant community mixtures

The mixtures of plant communities at the CBH and TLB sites revealed patterns in the drought response (i.e. here approximated with  $\Delta\text{WDI}$ ) between 2020 and 2021. High-centered polygons (HP) and tussock-sedge (TS) communities at the CBH site had a higher  $\Delta\text{WDI}$  when they were relatively more abundant in a  $5\text{ m} \times 5\text{ m}$  grid cell (figure 4). Both high-centered polygon communities at the CBH site (figure 4) and TLB site (figure S14(a)) demonstrated a bell-shaped behavior, e.g. low fCover of dry sedge and lichen-dominated communities (HP1) had both weak and strong increases in WDI, suggesting a consistent drought response across both sites. Conversely, grid cells with wet sedge and sphagnum-dominated communities (LW1) displayed a more

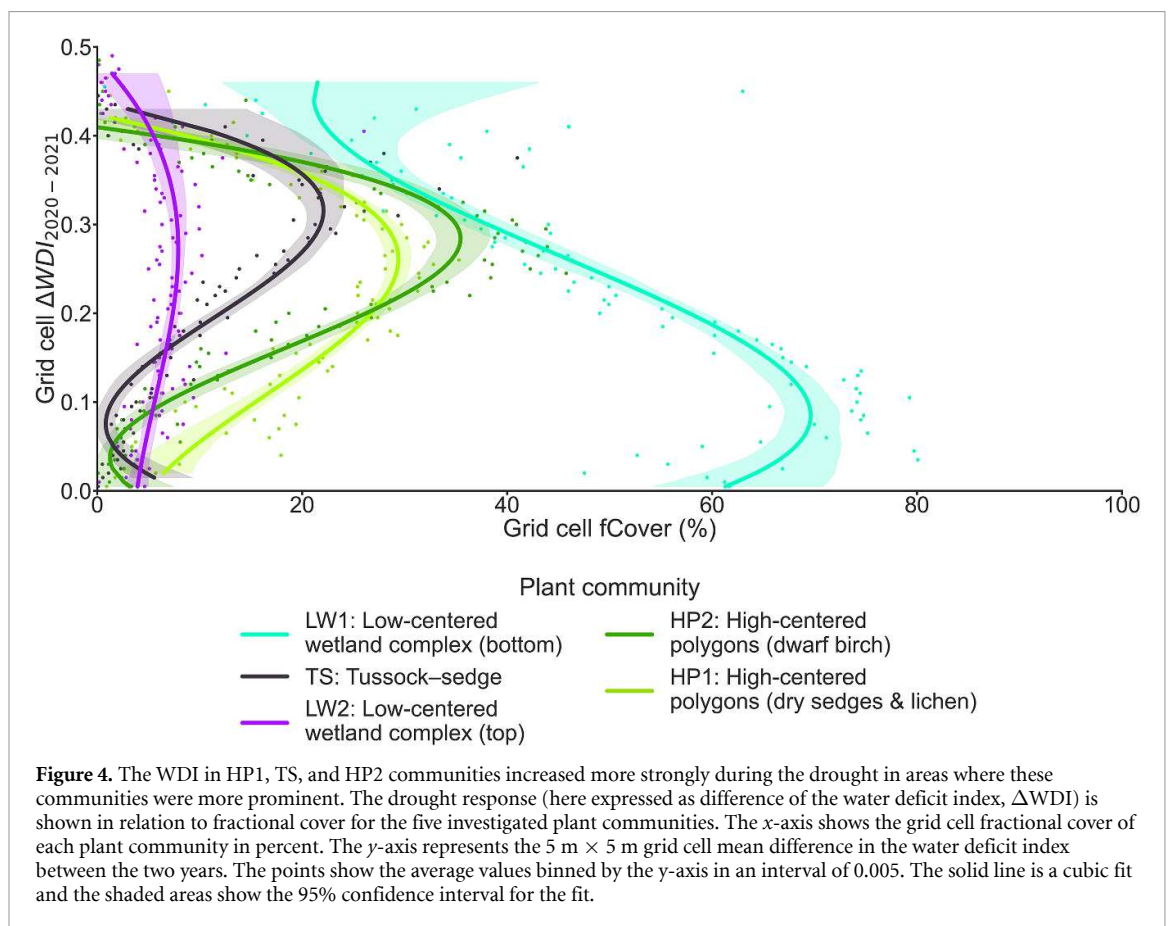
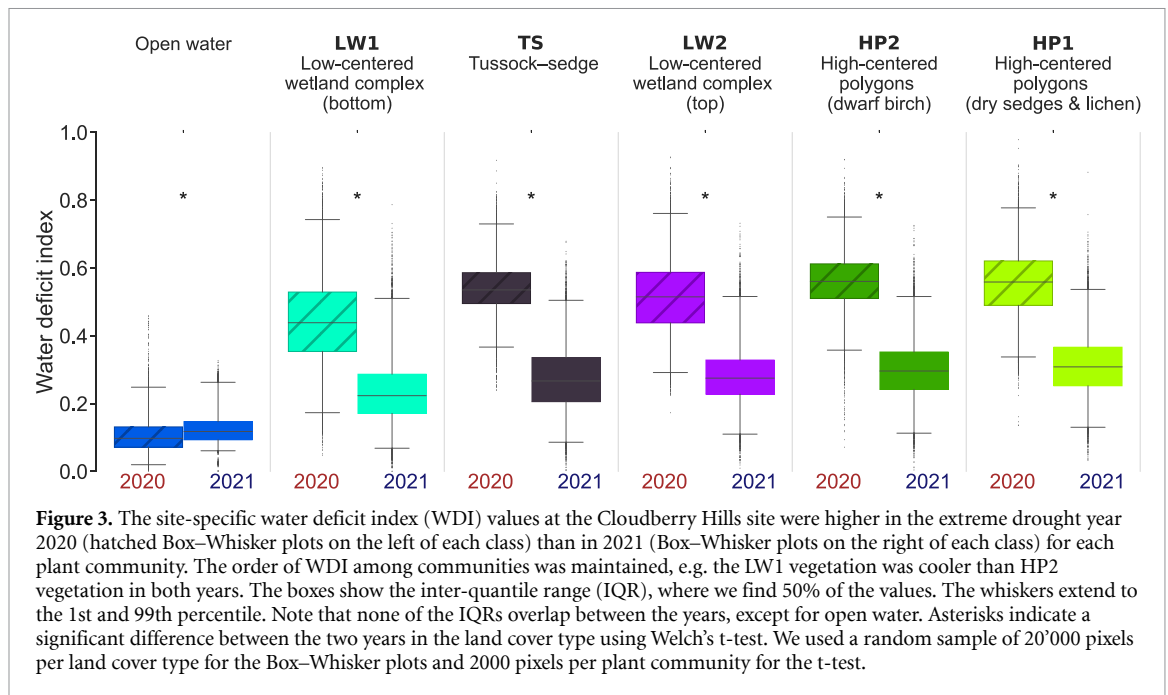


linear relationship between  $\Delta WDI$  and  $fCover$  at the CBH site, i.e. drought response weakened with a higher  $fCover$  of such communities (figure 4). The LW2 communities at the CBH site (figure 4) experienced the entire range of  $\Delta WDI$  over a constantly low  $fCover$ . Similarly, tussock-sedge communities at the Ridge site experienced a wide range of  $WDI$  change over a constantly high  $fCover$  in figure S14b.

#### 4. Discussion

Permafrost landscapes in the North-Eastern Siberian Arctic are undergoing amplified warming and face adverse effects from extreme events like summer droughts (Walsh *et al* 2020, Rantanen *et al* 2022). Based on high-resolution drone thermal and multispectral imagery, we found variations in  $\Delta T_{surf-air}$  of up to 3.6  $^{\circ}C$ , a proxy for land surface cooling,





between tundra plant community types at the Kytalyk research site during the reference (2021) and drought year (2020). Our results showed reduced land surface cooling of the studied plant communities during the

drought year, and that community mixture can have a mediating effect on drought responses. These results further our understanding of how drought responses of tundra plants vary across communities and space.

#### 4.1. Spatial variation in land surface cooling across tundra plant communities

We found that  $\Delta T_{\text{surf-air}}$  among plant communities differed by as much as 3.6 °C, indicating substantial spatial variation of land surface cooling across the landscape at the study sites. This variation is likely linked to topography and the related soil moisture (Kelly *et al* 2021, Yang *et al* 2021), plant physiology and canopy functioning (Michaletz *et al* 2015, Still *et al* 2021). The land surface cooling was mostly around 2 °C and up to 3.6 °C stronger in low-centered wetland complex communities compared to high-centered polygon communities. Similar localized cooling contrasts were observed at the Kytalyk research site, where areas of wet sedges had cooler  $T_{\text{air}}$  (at 1.7 m above the surface) than dwarf shrub areas (Juszak *et al* 2016). A potential bias in  $\Delta T_{\text{surf-air}}$  could be introduced by using a single location (flux tower) for  $T_{\text{air}}$  compared to multiple stations. However, we used the commonly used 2 m air temperatures from the flux tower data to be consistent with Yang *et al* (2021).

The high spatial variation in land surface cooling persisted during the drought year 2020, with similar rankings of mean  $\Delta T_{\text{surf-air}}$  among plant communities as in 2021. However, there were overall decreased magnitudes and variations in land surface cooling during the drought year, potentially attributed to differences in meteorological conditions and time of day of the drone flights between the two years, necessitating normalization of  $\Delta T_{\text{surf-air}}$ .

#### 4.2. Landscape-wide reduction of land surface cooling

In 2020, the WDI showed significant increases by around 0.2 compared to 2021, surpassing the reference year's interquartile range. This suggests a notable decrease in land surface cooling during the drought and a shift towards a dominance of sensible heat flux. This may indicate a potential positive feedback between reduced land surface cooling and the intensification of heatwaves, resembling the 2010 heatwave and drought in Western Siberia (Hauser *et al* 2016).

The shift in WDI was consistent across communities, suggesting a landscape-wide drought impact while maintaining the spatial patterns observed in  $\Delta T_{\text{surf-air}}$ . The plant communities found at the bottom of low-polygonal complexes (LW1) still showed stronger cooling than other plant communities during the drought of 2020 (figures 3 and S12). The stronger cooling maintained even during drought conditions could indicate that these communities have longer lasting moisture supply, which could be facilitated by lateral flow of surface water and permafrost thaw, as observed in the Lena River Delta under normal summer conditions (Helbig *et al* 2013). The prolonged moisture supply and associated

cooling could further enable the maintenance of photosynthetic productivity of these communities during drought conditions. When a landscape is drying, permafrost thaw may be reduced through a reduction of soil thermal conductance and lower heat transfer through drier moss layers, both of which have been shown to exert strong control on the landscape-wide cooling at the Kytalyk site (Blok *et al* 2011, Liljedahl *et al* 2011). Yet, a supply of soil moisture from thawing permafrost may buffer heatwaves by enabling vegetation to contribute more to the surface cooling of the landscape (Liljedahl *et al* 2011). Open water surfaces consistently showed low WDI values in both years, indicating reliability of our normalization step of  $\Delta T_{\text{surf-air}}$  to account for different meteorological conditions and flight timings. However atmospheric effects due to wind direction and cloudiness might still be detectable after normalization, which could be minimized by ensuring reliable drone data acquisition (i.e. deploy thermal reference targets, flying during clear sky conditions).

#### 4.3. Drought impact integrated over community mixtures

Despite a landscape-wide reduction in land surface cooling, the spatial aggregation of plant communities influences their drought response. Wet sedge-dominated communities in low-centered wetland complexes (LW1) at the CBH site (figure 4) exhibited a strong link between their drought response ( $\Delta\text{WDI}$ ) and relative abundance, while high-centered polygon and tussock-sedge communities displayed a bell-shaped signal, indicating a potential 'transition zone' effect. This effect, proposed by (Yang *et al* 2021), suggests that a transition between communities affected the thermoregulation capacity. Moreover, the community mixture and topographic position collectively shape the magnitude of the WDI change. For instance, the low  $\Delta\text{WDI}$  for low fCover at the bottom of the bell-shaped curve for HP2 in figure 4 may suggest that the proximity of low-centered wetland complex communities buffered the drought response of HP2 in that grid cell. In contrast, higher  $\Delta\text{WDI}$  and low fCover at the top of the curve may be linked to a more elevated position in the landscape, associated with more nearby HP1 communities. We based these assumptions on a qualitative preliminary analysis described in the supplementary materials section 5.1 and figure S15.

Overall, the complexity of drought response is closely tied to the spatial mixture of communities. This spatial relation may contribute to the formation of larger fire areas by increasing landscape connectivity under drought conditions, as demonstrated in boreal peatlands by (Thompson *et al* 2019) or illustrated by (Schaepman-Strub and Kim 2022). High-resolution spaceborne imagery could approximate landscape connectivity with plant communities and

estimate resilience of landscapes to heatwaves in larger areas of the Arctic tundra. Still, the detection of thresholds where landscapes become connected would rely on spaceborne TIR sensors, which currently cannot capture such fine-scale signals.

#### 4.4. Towards a mechanistic understanding from plant to landscape

Despite newly emerging trends toward more extreme events in the Arctic region, our understanding of the change in drought occurrence is still uncertain (Meredith *et al* 2019, Walsh *et al* 2020). Identifying responses and feedbacks of tundra ecosystems to heatwaves and droughts is relevant, as such extreme events often precede intense wildfire seasons like in Siberia in 2020 (Loranty *et al* 2016, Masrur *et al* 2022, Talucci *et al* 2022). The question remains how land surface cooling develops within growing seasons and whether the temporal snapshots presented here hold true for other moisture regimes and atmospheric conditions. For that, we need higher temporal coverage throughout the growing season of radiometrically stable thermal imagery in combination with in situ measurements, to support future studies on how the response of vegetation to drought regulates disturbances like wildfires or permafrost thaw in the Arctic tundra. However, the logistics of field observations and drone imagery are a limiting factor for research on Arctic extreme events, with few published studies based on observational or opportunistic investigations (van Beest *et al* 2022). Future spaceborne TIR missions like TRISHNA, LSTM, or SBG (Gerhards *et al* 2019, Buffet *et al* 2021) with frequent revisits and higher spatial resolution could become a game-changer in research on droughts in difficult-to-access regions.

## 5. Conclusion

The North-Eastern Siberian lowland tundra experienced an extreme drought in the summer of 2020, accompanied by record-high numbers of wildfires. We find that different plant communities at Kytalyk showed strong variation of up to 3.6 °C in land surface cooling, where wetter low-centered wetland complex communities had stronger cooling abilities than communities associated with dry soils on high-centered polygons. All plant communities showed a decrease in land surface cooling during the drought year (2020), which may be attributed to stomatal closure as a mechanism to preserve water loss. The strength of drought responses varied among community mixtures and seemed to show a topographical dependence. Overall, the high spatial variation of land surface cooling and drought responses of plant communities may influence their susceptibility to wildfires. We conclude that thermal and multispectral

drone-based approaches are robust and sensitive to assess drought response of tundra plant communities on land surface cooling. Considering upcoming space-borne TIR missions, we advocate using TIR data to advance process understanding from tundra plant to ecosystem level under extreme events, and how these processes feed back to heatwaves, permafrost thaw and wildfires.

## Data availability statement

The code used for GLCM computation, image classification, statistical analysis, and plotting the figures is openly available on <https://github.com/nrietze/ArcticDroughtPaper>.

The data that support the findings of this study are openly available at the following URL/DOI: <https://zenodo.org/records/10372082>.

## Acknowledgments

N R and K N were supported through the TRISHNA Science and Electronics Contribution (T-SEC), ESA PRODEX Trishna T-SEC Project (PEA C4000133711). Drone data acquisition was supported by the University Research Priority Program on Global Change and Biodiversity of the University of Zurich and by the Swiss National Science Foundation (Grant No. 178753).

## Author contributions

N R and G S S conceived the research idea. G S S, E P acquired the drone data and collected the necessary data in the field supported by S V K and T C M. G H provided the flux tower data at the research site. N R and J J A carried out the investigation, N R completed the analysis and data visualization. N R, J J A, and G S S wrote the manuscript. J J A and G S S supervised N R during this study. We thank Gilles Boulet for the constructive suggestions and discussions. All authors contributed to the final version of the manuscript.

## Conflict of interest

The author declare no competing interests.

## ORCID iDs

Nils Rietze  <https://orcid.org/0000-0001-7232-7799>

Jakob J Assmann  <https://orcid.org/0000-0002-3492-8419>

Elena Plekhanova  <https://orcid.org/0000-0002-5727-9175>

Kathrin Naegeli  <https://orcid.org/0000-0003-2443-7154>

Alexander Damm  <https://orcid.org/0000-0001-8965-3427>  
 Sergey V Karsanaev  <https://orcid.org/0000-0002-4055-381X>  
 Geert Hensgens  <https://orcid.org/0000-0001-6511-7224>  
 Gabriela Schaepman-Strub  <https://orcid.org/0000-0002-4069-1884>

## References

- Beguieria S, Vicente-Serrano S M and Angulo-Martínez M 2010 A multiscalar global drought dataset: the SPEI base: a new gridded product for the analysis of drought variability and impacts *Bull. Am. Meteorol. Soc.* **91** 1351–6
- Berni J A J, Zarco-Tejada P J, Suárez L and Fereres E 2009 Thermal and narrowband multispectral remote sensing for vegetation monitoring from an unmanned aerial vehicle *IEEE Trans. Geosci. Remote Sens.* **47** 722–38
- Blok D, Heijmans M M P D, Schaepman-Strub G, van Ruijven J, Parmentier F J W, Maximov T C and Berendse F 2011 The cooling capacity of mosses: controls on water and energy fluxes in a Siberian tundra site *Ecosystems* **14** 1055–65
- Buffet L, Gamet P, Maisongrande P, Salcedo C and Crebassol P 2021 The TIR instrument on TRISHNA satellite: a precursor of high resolution observation missions in the thermal infrared domain *Proc. SPIE* **11852** 300–10
- Copernicus Sentinel data 2020 Copernicus Dataspace Browser (available at: <https://browser.dataspace.copernicus.eu>)
- Farella M M, Fisher J B, Jiao W, Key K B and Barnes M L 2022 Thermal remote sensing for plant ecology from leaf to globe *J. Ecol.* **110** 1996–2014
- Faye E, Rebaudo F, Yáñez-Cajo D, Cauvy-Fraunié S and Dangles O 2016 A toolbox for studying thermal heterogeneity across spatial scales: from unmanned aerial vehicle imagery to landscape metrics *Methods Ecol. Evol.* **7** 437–46
- Gerhards M, Schlerf M, Mallick K and Udelhoven T 2019 Challenges and future perspectives of multi-/hyperspectral thermal infrared remote sensing for crop water-stress detection: a review *Remote Sens.* **11** 1240
- Hauser M, Orth R and Seneviratne S I 2016 Role of soil moisture versus recent climate change for the 2010 heat wave in western Russia *Geophys. Res. Lett.* **43** 2819–26
- Helbig M, Boike J, Langer M, Schreiber P, Runkle B R K and Kutzbach L 2013 Spatial and seasonal variability of polygonal tundra water balance: Lena River Delta, northern Siberia (Russia) *Hydrogeol. J.* **21** 133–47
- Juszk J, Eugster W, Heijmans M M P D and Schaepman-Strub G 2016 Contrasting radiation and soil heat fluxes in Arctic shrub and wet sedge tundra *Biogeosciences* **13** 4049–64
- Katul G G, Oren R, Manzoni S, Higgins C and Parlange M B 2012 Evapotranspiration: a process driving mass transport and energy exchange in the soil-plant-atmosphere-climate system *Rev. Geophys.* **50** 3
- Kazakov K 2023 Spravochno-informatsionnyy portal “Pogoda i klimat” *Reference information portal “Weather and Climate”* (available at: [www.pogodaiklimat.ru/msummary.php?m=all&y=all&id=23256](http://www.pogodaiklimat.ru/msummary.php?m=all&y=all&id=23256))
- Kelly J, Kljun N, Eklundh L, Klemetsson L, Liljebadh B, Olsson P O, Weslien P and Xie X 2021 Modelling and upscaling ecosystem respiration using thermal cameras and UAVs: application to a peatland during and after a hot drought *Agric. For. Meteorol.* **300** 108330
- Kelly J, Kljun N, Olsson P-O, Mihai L, Liljebadh B, Weslien P, Klemetsson L and Eklundh L 2019 Challenges and best practices for deriving temperature data from an uncalibrated UAV thermal infrared camera *Remote Sens.* **11** 567
- Liljedahl A K, Hinzman L D, Harazono Y, Zona D, Tweedie C E, Hollister R D, Engstrom R and Oechel W C 2011 Nonlinear controls on evapotranspiration in Arctic coastal wetlands *Biogeosciences* **8** 3375–89
- Loranty M M, Lieberman-Cribbin W, Berner L T, Natali S M, Goetz S J, Alexander H D and Kholodov A L 2016 Spatial variation in vegetation productivity trends, fire disturbance, and soil carbon across Arctic-boreal permafrost ecosystems *Environ. Res. Lett.* **11** 095008
- Marchand F L, Verlinden M, Kockelbergh F, Graae B J, Beyens L and Nijs I 2006 Disentangling effects of an experimentally imposed extreme temperature event and naturally associated desiccation on Arctic tundra *Funct. Ecol.* **20** 917–28
- Masrur A, Taylor A, Harris L, Barnes J and Petrov A 2022 Topography, climate and fire history regulate wildfire activity in the Alaskan tundra *J. Geophys. Res. Biogeosci.* **127** e2021JG006608
- Meredith M et al 2019 Polar regions *IPCC Special Report on the Ocean and Cryosphere in a Changing Climate* pp 203–320 (available at: [www.cambridge.org/core/product/identifier/9781009157964%23c3/type/book\\_part](http://www.cambridge.org/core/product/identifier/9781009157964%23c3/type/book_part))
- Mesas-Carrascosa F J, Pérez-Porras F, de Larriva J E M, Frau C M, Agüera-Vega F, Carvajal-Ramírez F, Martínez-Carricondo P and García-Ferrer A 2018 Drift correction of lightweight microbolometer thermal sensors on-board unmanned aerial vehicles *Remote Sens.* **10** 615
- Michaletz S T, Weiser M D, Zhou J, Kaspari M, Helliker B R and Enquist B J 2015 Plant thermoregulation: energetics, trait–environment interactions, and carbon economics *Trends Ecol. Evol.* **30** 714–24
- Moran M, Clarke T, Inoue Y and Vidal A 1994 Estimating crop water deficit using the relation between surface–air temperature and spectral vegetation index *Remote Sens. Environ.* **49** 246–63
- Nedbal V, Láská K and Brom J 2020 Mitigation of Arctic tundra surface warming by plant evapotranspiration: complete energy balance component estimation using LANDSAT satellite data *Remote Sens.* **12** 3395
- Nill L, Ullmann T, Kneisel C, Sobiech-Wolf J and Baumhauer R 2019 Assessing spatiotemporal variations of Landsat land surface temperature and multispectral indices in the Arctic Mackenzie delta region between 1985 and 2018 *Remote Sens.* **11** 2329
- Oehri J et al 2022 Vegetation type is an important predictor of the Arctic summer land surface energy budget *Nat. Commun.* **13** 1–12
- Overland J E and Wang M 2021 The 2020 Siberian heat wave *Int. J. Climatol.* **41** E2341–6
- Parmentier F J W, Van Huissteden J, Van Der Molen M K, Schaepman-Strub G, Karsanaev S A, Maximov T C and Dolman A J 2011 Spatial and temporal dynamics in eddy covariance observations of methane fluxes at a tundra site in northeastern Siberia *J. Geophys. Res. Biogeosci.* **116** G03016
- Rantanen M, Karpechko A Y, Lipponen A, Nordling K, Hyvärinen O, Ruosteenoja K, Vihma T and Laaksonen A 2022 The Arctic has warmed nearly four times faster than the globe since 1979 *Commun. Earth Environ.* **3** 1–10
- Raynolds M K et al 2019 A raster version of the circumpolar Arctic vegetation map (CAVM) *Remote Sens. Environ.* **232** 111297
- Rietze N, Assmann J J, Plekhanova E, Naegeli K, Damm A, Maximov T, Karsanaev S, Hensgens G and Schaepman-Strub G 2024 Summer drought weakens land surface cooling of tundra vegetation *Zenodo* (<https://doi.org/10.5281/zenodo.7886425>)
- Schaepman-Strub G and Kim J S 2022 What set Siberia ablaze? *Science* **378** 944–5
- Slette I J, Post A K, Awad M, Even T, Punzalan A, Williams S, Smith M D and Knapp A K 2019 How ecologists define drought, and why we should do better *Glob. Change Biol.* **25** 3193–200
- Still C J, Rastogi B, Page G F M, Griffith D M, Sibley A, Schulze M, Hawkins L, Pau S, Detto M and Helliker B R 2021 Imaging canopy temperature: shedding (thermal) light on ecosystem processes *New Phytol.* **230** 1746–53
- Still C et al 2019 Thermal imaging in plant and ecosystem ecology: applications and challenges *Ecosphere* **10** e02768

- Talucci A C, Loranty M M and Alexander H D 2022 Siberian taiga and tundra fire regimes from 2001–2020 *Environ. Res. Lett.* **17** 025001
- Thompson D K, Simpson B N, Whitman E, Barber Q E and Parisien M A 2019 Peatland hydrological dynamics as a driver of landscape connectivity and fire activity in the boreal plain of Canada *Forests* **10** 534
- Thunberg S M, Walsh J E, Euskirchen E S, Redilla K and Rocha A V 2021 Surface moisture budget of tundra and boreal ecosystems in Alaska: variations and drivers *Polar Sci.* **29** 100685
- van Beest F M, Barry T, Christensen T, Heiðmarsson S, McLennan D and Schmidt N M 2022 Extreme event impacts on terrestrial and freshwater biota in the Arctic: a synthesis of knowledge and opportunities *Front. Environ. Sci.* **10** 1748
- Vicente-Serrano S M, Beguería S and López-Moreno J I 2010 A multiscalar drought index sensitive to global warming: the standardized precipitation evapotranspiration index *J. Clim.* **23** 1696–718
- Walsh J E, Ballinger T J, Euskirchen E S, Hanna E, Mård J, Overland J E, Tangen H and Vihma T 2020 Extreme weather and climate events in northern areas: a review *Earth Sci. Rev.* **209** 103324
- Yang D *et al* 2022 Remote sensing from unoccupied aerial systems: opportunities to enhance Arctic plant ecology in a changing climate *J. Ecol.* **00** 1–24
- Yang D, Meng R, Morrison B D, McMahon A, Hantson W, Hayes D J, Breen A L, Salmon V G and Serbin S P 2020 A multi-sensor unoccupied aerial system improves characterization of vegetation composition and canopy properties in the Arctic tundra *Remote Sens.* **12** 2638
- Yang D, Morrison B D, Hantson W, Breen A L, McMahon A, Li Q, Salmon V G, Hayes D J and Serbin S P 2021 Landscape-scale characterization of Arctic tundra vegetation composition, structure, and function with a multi-sensor unoccupied aerial system *Environ. Res. Lett.* **16** 085005
- Zona D *et al* 2022 Pan-Arctic soil moisture control on tundra carbon sequestration and plant productivity *Glob. Change Biol.* **29** 1267–81